

Communication

# Nitrogen-Doped Nickel Selenium Nanosheets for Highly Efficient Oxygen Evolution Reaction

Chen Cai <sup>1,†</sup>, Cunyuan Gao <sup>2,†</sup>, Shuai Lin <sup>1</sup> and Bin Cai <sup>2,\*</sup> <sup>1</sup> Shandong Institute of Non-Metallic Materials, Jinan 250031, China; caichenyihao@163.com (C.C.)<sup>2</sup> School of Chemistry and Chemical Engineering, Shandong University, Jinan 250100, China

\* Correspondence: bin.cai@sdu.edu.cn

† These authors contributed equally to this work.

**Abstract:** Transition metal selenides have garnered considerable attention in the field of electrocatalytic oxygen evolution reaction (OER). However, their OER performances still lag behind those of Ir-based materials due to limited exposed active sites, inefficient electron transfer and inadequate stability. In this study, we have successfully synthesized nitrogen-doped NiSe<sub>2</sub> nanosheets, which exhibit high efficiency and long-term stability for the OER, requiring only 320 mV to reach a current density of 10 mA cm<sup>-2</sup>. The nitrogen doping plays a crucial role in effectively regulating the work function and semiconductor characteristics of NiSe<sub>2</sub>, which facilitates the electron transport and optimizes the catalytic sites. Furthermore, the NiSe<sub>2</sub> nanosheets present a larger surface area with more exposed active sites, thus resulting in exceptional OER catalytic activity. The nitrogen-doped NiSe<sub>2</sub> nanosheets also display superior stability, maintaining a sustained current density throughout an 8-h OER operation.

**Keywords:** oxygen evolution reaction; electrocatalyst; nitrogen doping; work function

## 1. Introduction

The energy crisis and environmental pollution issues have emerged as significant obstacles to the rapid development of society [1,2]. Hydrogen energy has attracted widespread attention due to its high energy density and environmentally friendly characteristics [3,4]. In the process of electrochemical water electrolysis, the anodic oxygen evolution reaction (OER) plays a crucial role [5–10]. However, the OER proceeds at a relatively slow rate due to the complicated four-electron transfer process, which ultimately hampers the energy conversion efficiency of the entire water electrolysis system [11–15]. Currently, noble metals such as Ru- and Ir-based catalysts have exhibited high catalytic activity for the oxygen evolution reaction [16,17]. However, their practical application is hindered by their high cost and poor stability [18]. Therefore, there is an urgent need to develop high-performance and cost-effective OER electrocatalysts.

To address this challenge, researchers have turned their attention to first-row transition metal dichalcogenides (MX<sub>2</sub>: M = Fe, Co, Ni; X = S, Se) as promising OER electrocatalysts. These materials are composed of abundant and low-cost elements, making them economically viable alternatives [19–23]. It is worth noting that the OER activity of these catalysts is strongly influenced by the coordination environment and electronic structure of the active sites. Consequently, significant efforts have been dedicated to developing superior electrocatalysts that can enhance the reaction kinetics and decrease the overpotentials. Various strategies have been explored to enhance the intrinsic activity, including morphology and size optimization [24–26], composition control [20,21,27], heteroatom doping [28–30], defect engineering [22,23], and the construction of heterojunctions [31,32].

Among the diverse MX<sub>2</sub>-based electrocatalysts, NiSe<sub>2</sub> has garnered significant attention due to its intrinsic catalytic properties and the presence of eight electrons in the 3d



**Citation:** Cai, C.; Gao, C.; Lin, S.; Cai, B. Nitrogen-Doped Nickel Selenium Nanosheets for Highly Efficient Oxygen Evolution Reaction. *Catalysts* **2023**, *13*, 1317. <https://doi.org/10.3390/catal13101317>

Academic Editor: Kai Wang

Received: 25 July 2023

Revised: 31 August 2023

Accepted: 5 September 2023

Published: 22 September 2023



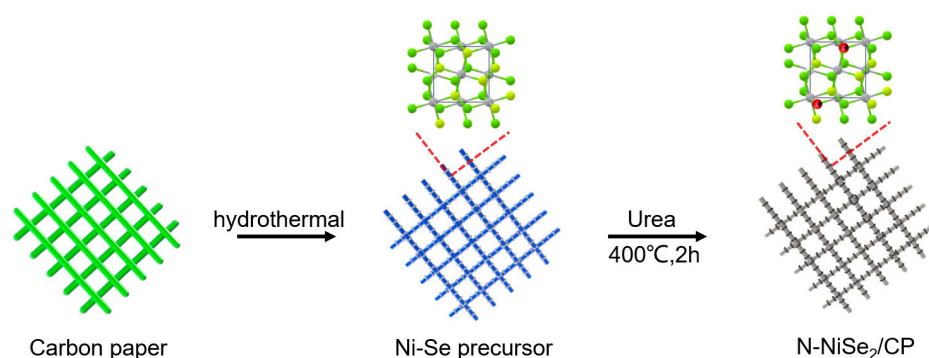
**Copyright:** © 2023 by the authors. Licensee MDPI, Basel, Switzerland. This article is an open access article distributed under the terms and conditions of the Creative Commons Attribution (CC BY) license (<https://creativecommons.org/licenses/by/4.0/>).

orbital, which enables facile regulation of its electronic structure [33,34]. However, the high resistance of NiSe<sub>2</sub>-based semiconductor materials significantly hampers their electrocatalytic performance. Recent studies have indicated that incorporating heteroatoms with higher electronegativity into the catalyst materials is an effective strategy for enhancing their activity. For instance, the incorporation of nitrogen into NiCo<sub>2</sub>S<sub>4</sub> nanowire arrays allows for the modulation of electron density and d-band center, resulting in high-efficient and stable electrocatalytic hydrogen evolution [35]. Nitrogen doping has also been employed to modify the electronic structure of Co<sub>2</sub>P nanorods to optimize the binding of water and hydrogen molecules, thus leading to enhanced the hydrogen evolution kinetics [36]. The substitution of stronger electronegative heteroatoms at anion sites effectively adjusts the electronic properties and weakens the interaction between the metal and anion [37,38]. Thus, the introduction of heteroatoms with higher electronegativity into the NiSe<sub>2</sub> lattices holds great promise for enhancing OER electrocatalysis.

Inspired by the above viewpoints, herein, we report nitrogen-doped NiSe<sub>2</sub> nanosheets on carbon paper (denoted as N-NiSe<sub>2</sub>/CP) toward high-efficiency and stable OER electrocatalysis in alkaline media. The lower work function of N-NiSe<sub>2</sub>/CP than that of undoped counterpart reveals that the introduction of nitrogen atoms can facilitate electron transport and improve the OER activity. Therefore, the as-prepared N-NiSe<sub>2</sub>/CP possesses largely improved OER activity compared with NiSe<sub>2</sub>/CP and N-CP, requiring only 320 mV to reach a current density of 10 mA cm<sup>-2</sup>. Impressively, the N-NiSe<sub>2</sub>/CP catalyst also displays superior stability for a long-term electrolysis up to 8 h. This work provides a promising prospect in designing highly active and stable electrocatalysts for water splitting.

## 2. Results and Discussion

The preparation procedure of N-NiSe<sub>2</sub> nanosheets on carbon paper was carried out as follows. Firstly, NiSe<sub>2</sub> precursor nanosheets were grown on carbon paper using a hydrothermal process (Scheme 1). The scanning electron microscopy (SEM) image (Figure S1) reveals the uniform and densely arranged growth of NiSe<sub>2</sub> nanosheets on the surface. To introduce nitrogen, the prepared NiSe<sub>2</sub> precursor nanosheets were immersed in a 0.5 M urea solution for 6 h. After drying, the sample was subjected to high-temperature calcination, resulting in the transformation of the NiSe<sub>2</sub> nanosheets into N-NiSe<sub>2</sub> nanosheets. As shown in Figure 1a,b, the N-NiSe<sub>2</sub> nanosheets remain the nanosheet structure, which not only increase the exposure of active sites for catalysis but also enhance their intimate contact with the electrolyte, resulting in the accelerated release of gaseous products. The phase composition of the catalysts was initially determined using X-ray diffraction (XRD). As shown in Figure 1c, pure NiSe<sub>2</sub>/CP and the N-NiSe<sub>2</sub>/CP exhibit one strong characteristic peak of carbon (PDF#26-1077) at 26.60°, which should be ascribed to the carbon paper. Other characteristic peaks belong to NiSe<sub>2</sub> (PDF#41-1495), and notably, nitrogen doping does not change the crystal structure of NiSe<sub>2</sub>. Furthermore, transmission electron microscopy (TEM) was conducted to investigate the nanostructure and elemental distribution of the N-NiSe<sub>2</sub>/CP. As shown in Figure 1d, the N-NiSe<sub>2</sub> nanosheets exhibit 2-dimensional structure with abundant overlapping interlaced ultrathin nanosheets. Figure 1e presents the high-resolution TEM (HR-TEM) image of the N-NiSe<sub>2</sub>/CP catalyst, revealing that the structural phase is preserved even after nitrogen doping. The lattice fringes with an interlayer spacing of 0.172 nm are attributed to the (222) plane of NiSe<sub>2</sub>. Figure 1f displays the elemental mapping images of C, N, Ni and Se obtained from energy dispersive X-ray (EDX) analysis of the N-NiSe<sub>2</sub>/CP, indicating the presence of these four elements throughout the nanosheets.



**Scheme 1.** Schematic illustration of the preparation procedure of N-NiSe<sub>2</sub>/CP.

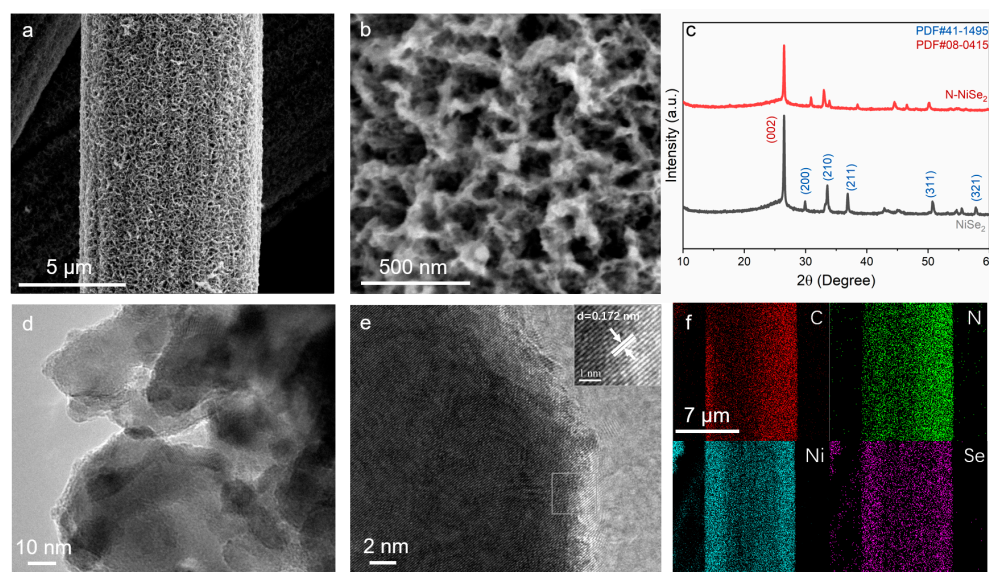


**Figure 1.** (a,b) The SEM images of the N-NiSe<sub>2</sub>/CP at different magnifications. (c) XRD pattern of NiSe<sub>2</sub>/CP and N-NiSe<sub>2</sub>/CP. (d,e) The TEM images of the N-NiSe<sub>2</sub>/CP at different magnifications. (f) EDX element maps of the N-NiSe<sub>2</sub>/CP.

In order to examine the impact of nitrogen on the surface composition and chemical valence states of the N-NiSe<sub>2</sub>/CP, X-ray photoelectron spectroscopy (XPS) analysis was performed on both the NiSe<sub>2</sub>/CP and N-NiSe<sub>2</sub>/CP. As shown in Figure 2a, the high-resolution XPS spectra of Ni 2p can be deconvoluted into two shakeup satellites (marked as “Sat.”) at 861.71 and 878.66 eV, two spin-orbit doublets of Ni<sup>2+</sup> at 853.91 and 871.44 eV as well as two spin-orbit doublets of Ni<sup>3+</sup> at 857.70 and 874.99 eV for the two electrodes. The Se 3d XPS spectrum of NiSe<sub>2</sub>/CP and N-NiSe<sub>2</sub>/CP is shown in Figure S4. The two prominent peaks at 53.6 eV for Se 3d<sub>5/2</sub> and 54.5 eV for Se 3d<sub>3/2</sub> indicate the existence of Se<sup>2-</sup> ions. Additionally, there is a shoulder peak at 58.0 eV and a weak peak at 55.5 eV, which can be assigned respectively to elemental Se-O and Se, owing to slight surface oxidation. Furthermore, the influence of nitrogen on the valence band center structures and work functions of the catalysts was investigated using ultraviolet photoemission spectroscopy (UPS). As shown in Figure 2b,c, the cutoff energy ( $E_{\text{cutoff}}$ ) values of NiSe<sub>2</sub> and N-NiSe<sub>2</sub> are determined to be 14.42 and 16.37 eV, respectively, while both the  $E_{\text{F}}$  are kept at 0 eV. Fermi level is the highest occupied energy level of fermions, which is defined as 0 eV. In this case, the work function ( $\Phi$ ) of NiSe<sub>2</sub> and N-NiSe<sub>2</sub> can be determined to be 6.78 and 4.83 eV versus vacuum via the formula,  $\Phi = h\nu - |E_{\text{cutoff}} - E_{\text{F}}|$ . As a result, these findings confirm that nitrogen doping effectively modulates the work function of NiSe<sub>2</sub>, leading to potential optimization of oxygen adsorption behaviors and enhanced electron transfer during the oxygen evolution reaction process. In order to further explore

the effect of nitrogen doping on the thickness of the nanosheets, we performed Atomic Force Microscopy (AFM) characterizations on both samples. As shown in Figure 3a,b, the thickness of the NiSe<sub>2</sub> nanosheets is estimated as 11.11 nm and their thickness increases to 11.49 nm after nitrogen doping.

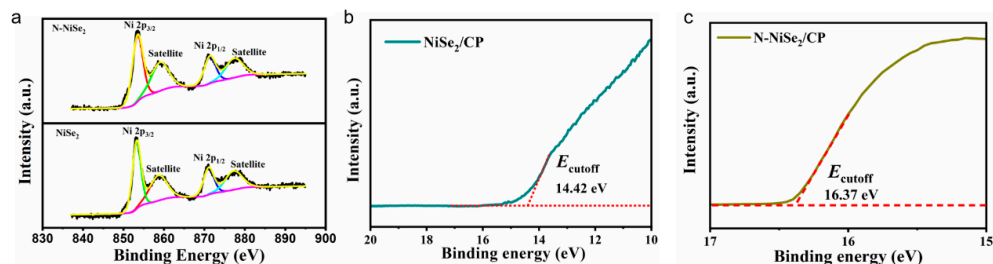


**Figure 2.** (a) High-resolution XPS spectra of Ni 2p. The cutoff energy ( $E_{\text{cutoff}}$ ) values for (b) NiSe<sub>2</sub>/CP and (c) N-NiSe<sub>2</sub>/CP are 16.37 and 14.42 eV, respectively.

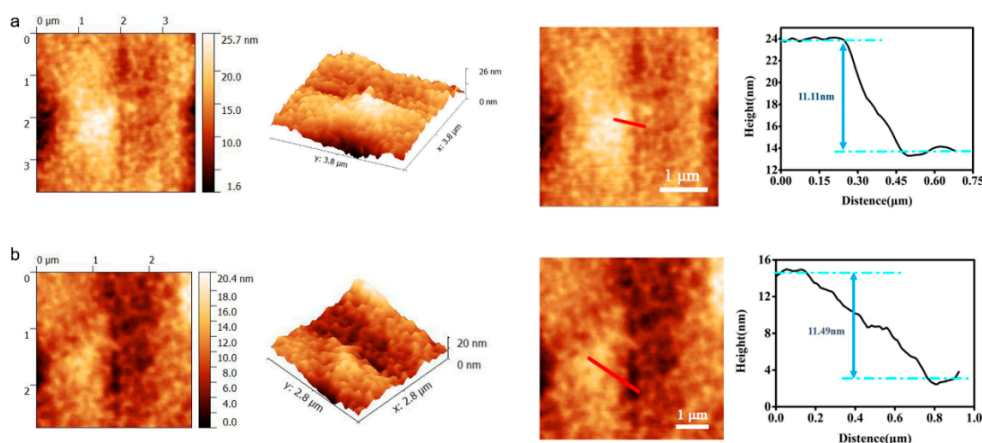


**Figure 3.** AFM phase images of (a) NiSe<sub>2</sub>/CP and (b) N-NiSe<sub>2</sub>/CP.

Their OER performances were assessed using a conventional three-electrode system in 1 M KOH solution. Figure 4a displays CV curves of as-prepared electrodes at a scan rate of 10 mV s<sup>-1</sup>. As anticipated, the N-NiSe<sub>2</sub>/CP electrode exhibits significantly lower overpotentials for achieving the same current densities compared to that of the NiSe<sub>2</sub>/CP and N-CP. The overpotential at a current density of 10 mA cm<sup>-2</sup> was only 320 mV, which is better than other previously reported non-noble catalysts (Table S1). In addition, the N-NiSe<sub>2</sub>/CP exhibits a smaller Tafel slope of 95 mV dec<sup>-1</sup> than that of the NiSe<sub>2</sub>/CP (198 mV dec<sup>-1</sup>) and N-CP (383 mV dec<sup>-1</sup>), further confirming a more favorable OER kinetics (Figure S5). Larger Tafel values indicate that the surface adsorption step has a dominant effect on the catalytic reaction rate. Electrochemical impedance spectroscopy (EIS) measurements were conducted to investigate the impact of nitrogen incorporation on the catalytic kinetics of the electrocatalysts. As shown in Figure 4b, the N-NiSe<sub>2</sub>/CP electrode exhibits a significantly lower charge-transfer resistance in comparison to the NiSe<sub>2</sub>/CP. This demonstrates the importance of nitrogen doping for facilitating the electron transfer and thus the reaction kinetics.

Stability represents a crucial parameter in the development of electrocatalysts, particularly for practical applications. Thus, a long-term stability measurement was performed at a constant potential of 1.6 V vs. RHE. The current density response of both the N-NiSe<sub>2</sub>/CP and NiSe<sub>2</sub>/CP electrodes is depicted in Figure S6. Remarkably, the N-NiSe<sub>2</sub>/CP exhibits exceptional stability throughout the 8-h runtime, highlighting its superior stability. To investigate the influence of nitrogen doping on the material properties, the Mott-Schottky (MS) measurement was conducted to determine the conductivity type of both N-NiSe<sub>2</sub>/CP and NiSe<sub>2</sub>/CP. Figure 4c presents the straight lines with positive and negative slopes

located in different potential regions, reflecting the coexistence of n- and p-type characteristics of NiSe<sub>2</sub>/CP. After nitrogen doping, the MS curves of N-NiSe<sub>2</sub>/CP exhibit linear characteristics with negative slopes across various potential regions, indicating its p-type semiconductor behavior. This effect positively influences electron transport, thereby leading to an enhanced catalytic efficiency.

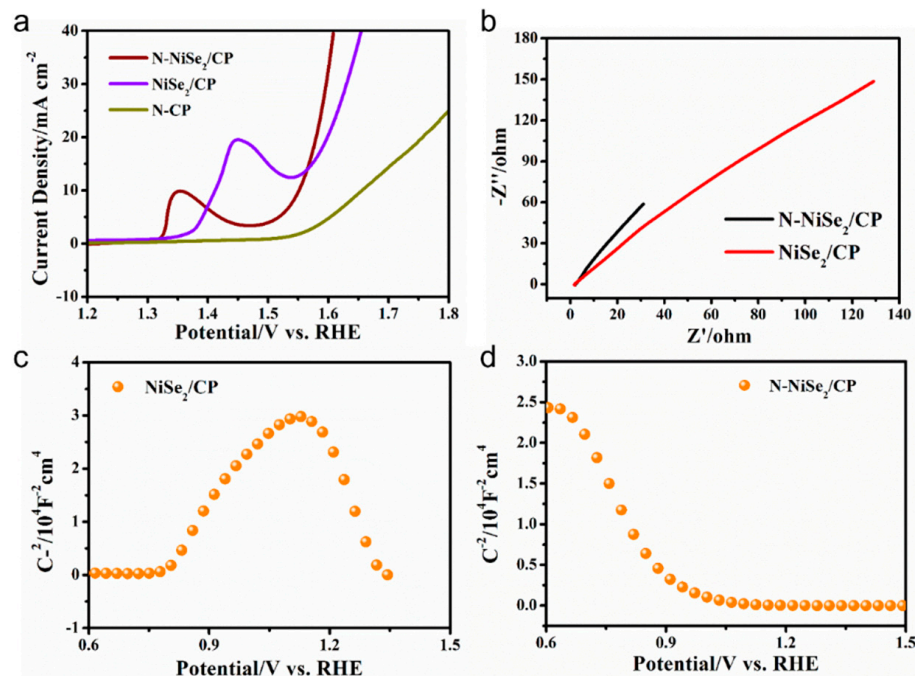


**Figure 4.** (a) The CV curves of the N-CP, NiSe<sub>2</sub>/CP and N-NiSe<sub>2</sub>/CP in 1 M KOH at a scan rate of 10 mV s<sup>-1</sup>. (b) EIS Nyquist plots of the NiSe<sub>2</sub>/CP and N-NiSe<sub>2</sub>/CP in 1 M KOH. M-S plot of (c) NiSe<sub>2</sub>/CP and (d) N-NiSe<sub>2</sub>/CP.

### 3. Materials and Methods

#### 3.1. Materials

Analytical-grade chemicals were employed in the experiment without any further purification. Nickel (II) sulfate hexahydrate, K<sub>2</sub>S<sub>2</sub>O<sub>8</sub>, ammonium hydroxide solution, selenium and urea were procured from McLean Biochemical Technology Co., Ltd., Shanghai, China. The Nafion solution was obtained from Sigma-Aldrich, St. Louis, MO, USA. Deionized water with a resistivity of 18.2 MΩ·cm was supplied by the Milli-Q water purification system.

#### 3.2. Ni Precursor Preparation

Nickel sulfate hexahydrate (5.26 g) and K<sub>2</sub>S<sub>2</sub>O<sub>8</sub> (1 g) were dissolved in deionized water (45 mL) and stirred for 10 min. Then, 3 mL of ammonia water was added dropwise and stirred for 30 s. After that, a piece of carbon paper (3.5 × 4.5 cm<sup>2</sup>) was added to the mixture. It was removed and rinsed after an hour.

#### 3.3. Synthesis of NiSe<sub>2</sub>/CP

NaBH<sub>4</sub> (38 mg), Se powder (39.5 mg) and deionized water (35 mL) were put into the Ni precursor and then hydrothermally heated at 180 °C for 24 h.

#### 3.4. Synthesis of N-NiSe<sub>2</sub>/CP

NiSe<sub>2</sub>/CP was soaked in 0.5 M urea for six hours, then calcined at 400 °C for 2 h under nitrogen atmosphere.

### 3.5. Material Characterizations

Scanning electron microscopy (SEM, FEI QUANTA FEG 250 field emission, produced by FEI, Hillsboro, OR, USA, secondary electron image resolution of 1.04 nm) was employed. The valence in the sample were obtained by X-ray photoelectron spectroscopy (XPS, PX13 0031 X-ray photoelectron spectroscopy analyzer, Bruker, Mannheim, Germany). X-ray diffraction (XRD) was performed on a SmartLab X-ray diffractometer from Rigaku, Japan, employing a Cu X-ray tube operated at a power of 9 kW. The valance band spectra were measured with a monochromatic He I light source (21.2 eV) and a VG Scienta R4000 analyzer. The work function ( $\phi$ ) was determined by the difference between the photon energy and the binding energy of the secondary cutoff edge.

### 3.6. Electrochemical Measurements

The electrochemical measurements were performed on a CHI 760E potentiostat. The Pt foil was used as counter electrode. The saturated calomel electrode (SCE) was used as the reference electrode. All potentials were converted into RHE according to the formula  $E_{\text{RHE}} = E_{\text{SCE}} + 0.059 \times \text{pH} + 0.242 \text{ V}$ .

## 4. Conclusions

We have successfully synthesized nitrogen-doped NiSe<sub>2</sub> nanosheets which are directly grown on carbon paper, demonstrating high-efficiency and long-term performance in the oxygen evolution reaction. The incorporation of nitrogen in NiSe<sub>2</sub> lattices leads to a lower work function and changes the semiconductor type, which enhances electron transport and improves OER activity. As a result, the N-NiSe<sub>2</sub>/CP electrode exhibits superior OER performance compared to the NiSe<sub>2</sub>/CP and N-CP electrode and the overpotential at a current density of 10 mA cm<sup>-2</sup> was only 320 mV. Notably, the N-NiSe<sub>2</sub>/CP also demonstrates excellent stability which sustains its electrocatalytic activity after an 8-h continuous operation. This work opens up promising prospects for designing highly active and stable electrocatalysts by heterometal substitution.

**Supplementary Materials:** The following supporting information can be downloaded at: <https://www.mdpi.com/article/10.3390/catal13101317/s1>, Figure S1. SEM images NiSe<sub>2</sub>/CP. Figure S2. SEM images N-NiSe<sub>2</sub>/CP. Figure S3. The corresponding lattice distance measurement data of N-NiSe<sub>2</sub>/CP. Figure S4. XPS spectra of the Se 3d. Figure S5. Tafel plots (potential versus log(current)) of different samples. Figure S6. Chronoamperometry measurement. Table S1. Comparison of the OER performance with other catalysts. References [39–54] are cited in the supplementary materials.

**Author Contributions:** Conceptualization, C.C. and B.C.; methodology, C.C., C.G., S.L. and B.C.; investigation, C.C., S.L. and C.G.; resources, C.C.; writing—original draft preparation, C.C. and C.G.; writing—review and editing, C.C., C.G. and B.C.; supervision, B.C.; funding acquisition, C.C. and B.C. All authors have read and agreed to the published version of the manuscript.

**Funding:** This research was funded by the Qilu Young Scholar Start-up Fund of Shandong University.

**Data Availability Statement:** Data are contained within the article.

**Conflicts of Interest:** The authors declare no conflict of interest.

## References

1. Yao, Y.; Hu, S.; Chen, W.; Huang, Z.-Q.; Wei, W.; Yao, T.; Liu, R.; Zang, K.; Wang, X.; Wu, G.; et al. Engineering the electronic structure of single atom Ru sites via compressive strain boosts acidic water oxidation electrocatalysis. *Nat. Catal.* **2019**, *2*, 304–313. [[CrossRef](#)]
2. Wu, Z.-Y.; Chen, F.-Y.; Li, B.; Yu, S.-W.; Finprock, Y.Z.; Meira, D.M.; Yan, Q.-Q.; Zhu, P.; Chen, M.-X.; Song, T.-W.; et al. Non-iridium-based electrocatalyst for durable acidic oxygen evolution reaction in proton exchange membrane water electrolysis. *Nat. Mater.* **2023**, *22*, 100–108. [[CrossRef](#)] [[PubMed](#)]
3. Benck, J.D.; Hellstern, T.R.; Kibsgaard, J.; Chakthranont, P.; Jaramillo, T.F. Catalyzing the Hydrogen Evolution Reaction (HER) with Molybdenum Sulfide Nanomaterials. *ACS Catal.* **2014**, *4*, 3957–3971. [[CrossRef](#)]
4. Yu, L.; Zhu, Q.; Song, S.; McElhenny, B.; Wang, D.; Wu, C.; Qin, Z.; Bao, J.; Yu, Y.; Chen, S.; et al. Non-noble metal-nitride based electrocatalysts for high-performance alkaline seawater electrolysis. *Nat. Commun.* **2019**, *10*, 5106. [[CrossRef](#)]

5. Seh, Z.W.; Kibsgaard, J.; Dickens, C.F.; Chorkendorff, I.; Nørskov, J.K.; Jaramillo, T.F. Combining theory and experiment in electrocatalysis: Insights into materials design. *Science* **2017**, *355*, eaad4998. [[CrossRef](#)]
6. Yu, J.; Garcés-Pineda, F.A.; González-Cobos, J.; Peña-Díaz, M.; Rogero, C.; Giménez, S.; Spadaro, M.C.; Arbiol, J.; Barja, S.; Galán-Mascarós, J.R. Sustainable oxygen evolution electrocatalysis in aqueous 1 M H<sub>2</sub>SO<sub>4</sub> with earth abundant nanostructured Co<sub>3</sub>O<sub>4</sub>. *Nat. Commun.* **2022**, *13*, 4341. [[CrossRef](#)]
7. Li, L.; Wang, P.; Shao, Q.; Huang, X. Recent Progress in Advanced Electrocatalyst Design for Acidic Oxygen Evolution Reaction. *Adv. Mater.* **2021**, *33*, 2004243. [[CrossRef](#)]
8. Zu, L.; Qian, X.; Zhao, S.; Liang, Q.; Chen, Y.E.; Liu, M.; Su, B.-J.; Wu, K.-H.; Qu, L.; Duan, L.; et al. Self-Assembly of Ir-Based Nanosheets with Ordered Interlayer Space for Enhanced Electrocatalytic Water Oxidation. *J. Am. Chem. Soc.* **2022**, *144*, 2208–2217. [[CrossRef](#)]
9. Logeshwaran, N.; Vijayapradeep, S.; Kim, A.R.; Sampath, P.; Ramakrishnan, S.; Poudel, M.B.; Kim, H.; Yoo, D.J. Study of engineering electronic structure modulated non-noble metal oxides for scaled-up alkaline blend seawater splitting. *J. Energy Chem.* **2023**, *86*, 167–179. [[CrossRef](#)]
10. Poudel, M.B.; Logeshwaran, N.; Kim, A.R.; Karthikeyan, S.C.; Vijayapradeep, S.; Yoo, D.J. Integrated core-shell assembly of Ni<sub>3</sub>S<sub>2</sub> nanowires and CoMoP nanosheets as highly efficient bifunctional electrocatalysts for overall water splitting. *J. Alloys Compd.* **2023**, *960*, 170678. [[CrossRef](#)]
11. Shi, Q.; Zhu, C.; Du, D.; Lin, Y. Robust noble metal-based electrocatalysts for oxygen evolution reaction. *Chem. Soc. Rev.* **2019**, *48*, 3181–3192. [[CrossRef](#)] [[PubMed](#)]
12. Chia, X.; Pumera, M. Characteristics and performance of two-dimensional materials for electrocatalysis. *Nat. Catal.* **2018**, *1*, 909–921. [[CrossRef](#)]
13. Kim, M.; Park, J.; Kang, M.; Kim, J.Y.; Lee, S.W. Toward Efficient Electrocatalytic Oxygen Evolution: Emerging Opportunities with Metallic Pyrochlore Oxides for Electrocatalysts and Conductive Supports. *ACS Cent. Sci.* **2020**, *6*, 880–891. [[CrossRef](#)]
14. Grimaud, A.; Diaz-Morales, O.; Han, B.; Hong, W.T.; Lee, Y.-L.; Giordano, L.; Storzinger, K.A.; Koper, M.T.M.; Shao-Horn, Y. Activating lattice oxygen redox reactions in metal oxides to catalyze oxygen evolution. *Nat. Chem.* **2017**, *9*, 457–465. [[CrossRef](#)] [[PubMed](#)]
15. Zhao, S.; Tan, C.; He, C.-T.; An, P.; Xie, F.; Jiang, S.; Zhu, Y.; Wu, K.-H.; Zhang, B.; Li, H.; et al. Structural transformation of highly active metal-organic framework electrocatalysts during the oxygen evolution reaction. *Nat. Energy* **2020**, *5*, 881–890. [[CrossRef](#)]
16. Feng, J.; Lv, F.; Zhang, W.; Li, P.; Wang, K.; Yang, C.; Wang, B.; Yang, Y.; Zhou, J.; Lin, F.; et al. Iridium-Based Multimetallic Porous Hollow Nanocrystals for Efficient Overall-Water-Splitting Catalysis. *Adv. Mater.* **2017**, *29*, 1703798. [[CrossRef](#)]
17. Reier, T.; Pawolek, Z.; Cherevko, S.; Bruns, M.; Jones, T.; Teschner, D.; Selve, S.; Bergmann, A.; Nong, H.N.; Schlögl, R.; et al. Molecular Insight in Structure and Activity of Highly Efficient, Low-Ir Ir-Ni Oxide Catalysts for Electrochemical Water Splitting (OER). *J. Am. Chem. Soc.* **2015**, *137*, 13031–13040. [[CrossRef](#)]
18. Xue, S.; Deng, W.; Yang, F.; Yang, J.; Amiin, I.S.; He, D.; Tang, H.; Mu, S. Hexapod PtRuCu Nanocrystalline Alloy for Highly Efficient and Stable Methanol Oxidation. *ACS Catal.* **2018**, *8*, 7578–7584. [[CrossRef](#)]
19. Suen, N.-T.; Hung, S.-F.; Quan, Q.; Zhang, N.; Xu, Y.-J.; Chen, H.M. Electrocatalysis for the oxygen evolution reaction: Recent development and future perspectives. *Chem. Soc. Rev.* **2017**, *46*, 337–365. [[CrossRef](#)]
20. Fang, L.; Li, W.; Guan, Y.; Feng, Y.; Zhang, H.; Wang, S.; Wang, Y. Tuning Unique Peapod-Like Co(S<sub>x</sub>Se<sub>1-x</sub>)<sub>2</sub> Nanoparticles for Efficient Overall Water Splitting. *Adv. Funct. Mater.* **2017**, *27*, 1701008. [[CrossRef](#)]
21. Xu, X.; Liang, H.; Ming, F.; Qi, Z.; Xie, Y.; Wang, Z. Prussian Blue Analogues Derived Penroseite (Ni,Co)Se<sub>2</sub> Nanocages Anchored on 3D Graphene Aerogel for Efficient Water Splitting. *ACS Catal.* **2017**, *7*, 6394–6399. [[CrossRef](#)]
22. Yan, D.; Li, Y.; Huo, J.; Chen, R.; Dai, L.; Wang, S. Defect Chemistry of Nonprecious-Metal Electrocatalysts for Oxygen Reactions. *Adv. Mater.* **2017**, *29*, 1606459. [[CrossRef](#)]
23. Liu, Y.; Cheng, H.; Lyu, M.; Fan, S.; Liu, Q.; Zhang, W.; Zhi, Y.; Wang, C.; Xiao, C.; Wei, S.; et al. Low Overpotential in Vacancy-Rich Ultrathin CoSe<sub>2</sub> Nanosheets for Water Oxidation. *J. Am. Chem. Soc.* **2014**, *136*, 15670–15675. [[CrossRef](#)] [[PubMed](#)]
24. Gao, R.; Zhang, H.; Yan, D. Iron diselenide nanoplatelets: Stable and efficient water-electrolysis catalysts. *Nano Energy* **2017**, *31*, 90–95. [[CrossRef](#)]
25. Liu, X.; Liu, Y.; Fan, L.-Z. MOF-derived CoSe<sub>2</sub> microspheres with hollow interiors as high-performance electrocatalysts for the enhanced oxygen evolution reaction. *J. Mater. Chem. A* **2017**, *5*, 15310–15314. [[CrossRef](#)]
26. You, B.; Sun, Y. Hierarchically Porous Nickel Sulfide Multifunctional Superstructures. *Adv. Energy Mater.* **2016**, *6*, 1502333. [[CrossRef](#)]
27. Zhang, J.; Wu, M.-H.; Shi, Z.-T.; Jiang, M.; Jian, W.-J.; Xiao, Z.; Li, J.; Lee, C.-S.; Xu, J. Composition and Interface Engineering of Alloyed MoS<sub>2</sub>xSe<sub>2</sub>(1-x) Nanotubes for Enhanced Hydrogen Evolution Reaction Activity. *Small* **2016**, *12*, 4379–4385. [[CrossRef](#)] [[PubMed](#)]
28. Liu, H.; He, Q.; Jiang, H.; Lin, Y.; Zhang, Y.; Habib, M.; Chen, S.; Song, L. Electronic Structure Reconfiguration toward Pyrite NiS<sub>2</sub> via Engineered Heteroatom Defect Boosting Overall Water Splitting. *ACS Nano* **2017**, *11*, 11574–11583. [[CrossRef](#)]
29. Hao, J.; Yang, W.; Hou, J.; Mao, B.; Huang, Z.; Shi, W. Nitrogen doped NiS<sub>2</sub> nanoarrays with enhanced electrocatalytic activity for water oxidation. *J. Mater. Chem. A* **2017**, *5*, 17811–17816. [[CrossRef](#)]
30. Dong, Q.; Wang, Q.; Dai, Z.; Qiu, H.; Dong, X. MOF-Derived Zn-Doped CoSe<sub>2</sub> as an Efficient and Stable Free-Standing Catalyst for Oxygen Evolution Reaction. *ACS Appl. Mater. Inter.* **2016**, *8*, 26902–26907. [[CrossRef](#)]

31. Yin, J.; Li, Y.; Lv, F.; Lu, M.; Sun, K.; Wang, W.; Wang, L.; Cheng, F.; Li, Y.; Xi, P.; et al. Oxygen Vacancies Dominated NiS<sub>2</sub>/CoS<sub>2</sub> Interface Porous Nanowires for Portable Zn–Air Batteries Driven Water Splitting Devices. *Adv. Mater.* **2017**, *29*, 1704681. [[CrossRef](#)] [[PubMed](#)]
32. Wang, X.; Zhuang, L.; Jia, Y.; Liu, H.; Yan, X.; Zhang, L.; Yang, D.; Zhu, Z.; Yao, X. Plasma-Triggered Synergy of Exfoliation, Phase Transformation, and Surface Engineering in Cobalt Diselenide for Enhanced Water Oxidation. *Angew. Chem. Int. Ed.* **2018**, *57*, 16421–16425. [[CrossRef](#)] [[PubMed](#)]
33. Zhou, W.; Wu, X.-J.; Cao, X.; Huang, X.; Tan, C.; Tian, J.; Liu, H.; Wang, J.; Zhang, H. Ni<sub>3</sub>S<sub>2</sub> nanorods/Ni foam composite electrode with low overpotential for electrocatalytic oxygen evolution. *Energy Environ. Sci.* **2013**, *6*, 2921–2924. [[CrossRef](#)]
34. Xu, K.; Chen, P.; Li, X.; Tong, Y.; Ding, H.; Wu, X.; Chu, W.; Peng, Z.; Wu, C.; Xie, Y. Metallic Nickel Nitride Nanosheets Realizing Enhanced Electrochemical Water Oxidation. *J. Am. Chem. Soc.* **2015**, *137*, 4119–4125. [[CrossRef](#)]
35. Wu, Y.; Liu, X.; Han, D.; Song, X.; Shi, L.; Song, Y.; Niu, S.; Xie, Y.; Cai, J.; Wu, S.; et al. Electron density modulation of NiCo<sub>2</sub>S<sub>4</sub> nanowires by nitrogen incorporation for highly efficient hydrogen evolution catalysis. *Nat. Commun.* **2018**, *9*, 1425. [[CrossRef](#)]
36. Men, Y.; Li, P.; Zhou, J.; Cheng, G.; Chen, S.; Luo, W. Tailoring the Electronic Structure of Co<sub>2</sub>P by N Doping for Boosting Hydrogen Evolution Reaction at All pH Values. *ACS Catal.* **2019**, *9*, 3744–3752. [[CrossRef](#)]
37. Men, Y.; Li, P.; Yang, F.; Cheng, G.; Chen, S.; Luo, W. Nitrogen-doped CoP as robust electrocatalyst for high-efficiency pH-universal hydrogen evolution reaction. *Appl. Catal. B-Environ.* **2019**, *253*, 21–27. [[CrossRef](#)]
38. Li, F.; Han, G.-E.; Noh, H.-J.; Jeon, J.-P.; Ahmad, I.; Chen, S.; Yang, C.; Bu, Y.; Fu, Z.; Lu, Y.; et al. Balancing hydrogen adsorption/desorption by orbital modulation for efficient hydrogen evolution catalysis. *Nat. Commun.* **2019**, *10*, 4060. [[CrossRef](#)]
39. Wen, T.; Zheng, Y.; Zhang, J.; Davey, K.; Qiao, S.-Z. Co (II) Boron Imidazolite Framework with Rigid Auxiliary Linkers for Stable Electrocatalytic Oxygen Evolution Reaction. *Adv. Sci.* **2019**, *6*, 1801920. [[CrossRef](#)]
40. Guo, H.; Feng, Q.; Zhu, J.; Xu, J.; Li, Q.; Liu, S.; Xu, K.; Zhang, C.; Liu, T. Cobalt nanoparticle-embedded nitrogen-doped carbon/carbon nanotube frameworks derived from a metal–organic framework for tri-functional ORR, OER and HER electrocatalysis. *J. Mater. Chem. A* **2019**, *7*, 3664–3672. [[CrossRef](#)]
41. Wu, Y.; Qiu, X.; Liang, F.; Zhang, Q.; Koo, A.; Dai, Y.; Lei, Y.; Sun, X. A metal-organic framework-derived bifunctional catalyst for hybrid sodium-air batteries. *Appl. Catal. B-Environ.* **2019**, *241*, 407–414. [[CrossRef](#)]
42. Xu, H.; Shi, Z.-X.; Tong, Y.-X.; Li, G.-R. Porous Microrod Arrays Constructed by Carbon-Confined NiCo@NiCoO<sub>2</sub> Core@Shell Nanoparticles as Efficient Electrocatalysts for Oxygen Evolution. *Adv. Mater.* **2018**, *30*, 1705442. [[CrossRef](#)] [[PubMed](#)]
43. Jiang, Y.; Deng, Y.-P.; Fu, J.; Lee, D.U.; Liang, R.; Cano, Z.P.; Liu, Y.; Bai, Z.; Hwang, S.; Yang, L.; et al. Interpenetrating Triphase Cobalt-Based Nanocomposites as Efficient Bifunctional Oxygen Electrocatalysts for Long-Lasting Rechargeable Zn–Air Batteries. *Adv. Energy Mater.* **2018**, *8*, 1702900. [[CrossRef](#)]
44. Li, Y.; Jia, B.; Fan, Y.; Zhu, K.; Li, G.; Su, C.-Y. Bimetallic Zeolitic Imidazolate Framework Derived Carbon Nanotubes Embedded with Co Nanoparticles for Efficient Bifunctional Oxygen Electrocatalyst. *Adv. Energy Mater.* **2018**, *8*, 1702048. [[CrossRef](#)]
45. Yan, G.; Lian, Y.; Gu, Y.; Yang, C.; Sun, H.; Mu, Q.; Li, Q.; Zhu, W.; Zheng, X.; Chen, M.; et al. Phase and Morphology Transformation of MnO<sub>2</sub> Induced by Ionic Liquids toward Efficient Water Oxidation. *ACS Catal.* **2018**, *8*, 10137–10147. [[CrossRef](#)]
46. Wang, X.; Huang, X.; Gao, W.; Tang, Y.; Jiang, P.; Lan, K.; Yang, R.; Wang, B.; Li, R. Metal–organic framework derived CoTe<sub>2</sub> encapsulated in nitrogen-doped carbon nanotube frameworks: A high-efficiency bifunctional electrocatalyst for overall water splitting. *J. Mater. Chem. A* **2018**, *6*, 3684–3691. [[CrossRef](#)]
47. Xu, J.; Zhang, H.; Xu, P.; Wang, R.; Tong, Y.; Lu, Q.; Gao, F. In situ construction of hierarchical Co/MnO@graphite carbon composites for highly supercapacitive and OER electrocatalytic performances. *Nanoscale* **2018**, *10*, 13702–13712. [[CrossRef](#)]
48. Qin, Q.; Zhang, G.; Chai, Z.; Zhang, J.; Cui, Y.; Li, T.; Zheng, W. Ionic liquid-assisted synthesis of Cu<sub>7</sub>Te<sub>4</sub> ultrathin nanosheets with enhanced electrocatalytic activity for water oxidation. *Nano Energy* **2017**, *41*, 780–787. [[CrossRef](#)]
49. He, P.; Yu, X.-Y.; Lou, X.W. Carbon-Incorporated Nickel–Cobalt Mixed Metal Phosphide Nanoboxes with Enhanced Electrocatalytic Activity for Oxygen Evolution. *Angew. Chem. Int. Ed.* **2017**, *56*, 3897–3900. [[CrossRef](#)]
50. Xi, W.; Ren, Z.; Kong, L.; Wu, J.; Du, S.; Zhu, J.; Xue, Y.; Meng, H.; Fu, H. Dual-valence nickel nanosheets covered with thin carbon as bifunctional electrocatalysts for full water splitting. *J. Mater. Chem. A* **2016**, *4*, 7297–7304. [[CrossRef](#)]
51. Zhang, Q.; Wang, Y.; Wang, Y.; Al-Enizi, A.M.; Elzatahry, A.A.; Zheng, G. Myriophyllum-like hierarchical TiN@Ni<sub>3</sub>N nanowire arrays for bifunctional water splitting catalysts. *J. Mater. Chem. A* **2016**, *4*, 5713–5718. [[CrossRef](#)]
52. Liu, Q.; Wang, Y.; Dai, L.; Yao, J. Scalable Fabrication of Nanoporous Carbon Fiber Films as Bifunctional Catalytic Electrodes for Flexible Zn–Air Batteries. *Adv. Mater.* **2016**, *28*, 3000–3006. [[CrossRef](#)] [[PubMed](#)]
53. Hou, Y.; Wen, Z.; Cui, S.; Ci, S.; Mao, S.; Chen, J. An Advanced Nitrogen-Doped Graphene/Cobalt-Embedded Porous Carbon Polyhedron Hybrid for Efficient Catalysis of Oxygen Reduction and Water Splitting. *Adv. Funct. Mater.* **2015**, *25*, 872–882. [[CrossRef](#)]
54. Feng, L.-L.; Yu, G.; Wu, Y.; Li, G.-D.; Li, H.; Sun, Y.; Asefa, T.; Chen, W.; Zou, X. High-Index Faceted Ni<sub>3</sub>S<sub>2</sub> Nanosheet Arrays as Highly Active and Ultrastable Electrocatalysts for Water Splitting. *J. Am. Chem. Soc.* **2015**, *137*, 14023–14026. [[CrossRef](#)]

**Disclaimer/Publisher’s Note:** The statements, opinions and data contained in all publications are solely those of the individual author(s) and contributor(s) and not of MDPI and/or the editor(s). MDPI and/or the editor(s) disclaim responsibility for any injury to people or property resulting from any ideas, methods, instructions or products referred to in the content.